Transport in Porous Media
https://doi.org/10.1007/s11242-018-1155-6

Anomalous Dispersion in Pore-Scale Simulations of Two-Phase Flow

Dimetre Triadis[1] · **Fei Jiang**[2,3,4] · **Diogo Bolster**[5]

Received: 25 January 2018 / Accepted: 24 August 2018

Abstract
We investigate anomalous dispersion in steady-state two-phase flow though a random, artificial porous domain. A natural distribution of trapped wetting-phase fluid was obtained via two-phase lattice Boltzmann drainage simulations. To avoid spurious velocities, accurate inter-pore velocity fields were derived via additional one-phase lattice Boltzmann simulations incorporating slip boundary conditions imposed at various interfaces. The nature of the active dispersion at various timescales was subsequently studied via random walk particle tracking. For our system, results show persistent anomalous dispersion that depends strongly on the assumed molecular diffusivity and the initial positions of tracer particles. Imposing slip versus no-slip boundary conditions on fluid–fluid interfaces made no observable difference to results, indicating that observed anomalous dispersion resulted primarily from the complex flow network induced by the trapped fluid phase.

Keywords Multiphase flow · Anomalous transport

1 Introduction

Multiphase flows through porous media are of broad interest in many natural, engineered and hybrid environments. Examples include geologic sequestration of carbon dioxide (Bachu 2000), hydrocarbon extraction (Lake 1989), irrigation and rainfall infiltration through soils (Daly and Porporato 2005), artificial aquifer recharge (Bouwer 2002), nuclear waste repositories (Berglund et al. 2013), biochemical reactors (Fernández-Arévalo et al. 2014), remediation of contaminated soils (Mercer and Cohen 1990) and fuel cell technology (Berning and Dji-

✉ Dimetre Triadis
triadis@imi.kyushu-u.ac.jp

1 Institute of Mathematics for Industry, Kyushu University, Fukuoka, Japan

2 Department of Mechanical Engineering, Yamaguchi University, Ube, Japan

3 CO2 Storage Division, International Institute for Carbon-Neutral Energy Research (WPI-I2CNER), Kyushu University, Fukuoka, Japan

4 Blue energy center for SGE technology (BEST), Yamaguchi University, Ube, Japan

5 Department of Civil and Environmental Engineering and Earth Sciences, University of Notre Dame, Notre Dame, IN, USA

Published online: 04 October 2018

lali 2003) among many others. Flows across these systems can vary greatly, for example spanning the full spectrum from viscous dominated laminar flows to inertially dominated turbulent flows (e.g., Sund et al. 2015). However, all flows through porous media have the common feature of the presence of a solid matrix whose boundaries exert no slip conditions that are distributed throughout the entire domain, giving rise to a potentially broad distribution of velocity scales (Bijeljic et al. 2013b). These features already exist for single-phase systems, but when two or more fluid phases are present, an additional level of complexity arises. The presence of multiple fluid phases also fundamentally influences the way dissolved substances move through the porous medium. For example, if one of the phases is trapped, as is common, the flow path structure through the porous medium is altered. This in turn impacts spreading and mixing (Dentz et al. 2011) dynamics, which are physical processes that must be understood for example in the context of risk assessment (de Barros et al. 2011) and remediation efforts (de Barros et al. 2013).

Anomalous transport, as typically quantified by the non-Fickian time-scaling of spreading ($\sigma^2 \sim t^\beta$, $\beta \neq 1$), is ubiquitous in porous media, having been observed all the way from the smallest scales on the order of mm in pores (Bijeljic and Blunt 2006; Bijeljic et al. 2013b) to larger scales on the order of 100s of meters and more in aquifers (Gómez-Hernández et al. 2017). Such anomalous behavior is typically associated with long jumps that occur due to the presence of persistent preferential flow paths (e.g., Zhang and Benson 2008) and/or persistent long waiting times in immobile regions of a porous medium, that occur for example due to the presence of dead end pores or very low conductivity flow regions (Berkowitz et al. 2006). This is also typically reflected in the intermittent nature of particle transport, where particles persist in regimes of fast or slow speeds and acceleration, which has been observed in synthetic 2D porous media (De Anna et al. 2013) as well as real complex 3D porous structures (Kang et al. 2014). Depending on the scales of interest, these anomalous scalings can be a reflection of pre-asymptotic behavior that eventually converges to Fickian once all relevant scales have been sampled, typically via diffusion (Taylor 1953). The time scale for this to happen is on the order of $\tau_D = L^2/D$, where L is a characteristic length associated with the medium of interest and D is the diffusion coefficient. Such asymptotic behavior can be well predicted by theories such as the method of moments (Brenner 2013) or volume averaging (Whitaker 2013), but this asymptotic timescale may be prohibitively large. Additionally pre-asymptotic volume averaging models can predict components of the anomalous transport regime (e.g., Wood 2007; Bolster et al. 2011), but still typically need a known characteristic length scale L with which to make assumptions required to close the problem. The resulting upscaled effective equations tend to be nonlocal in time with tempering effects kicking in after the characteristic diffusion time τ_D. When no clear length scale L exists, anomalous behavior can persist indefinitely (Schumer et al. 2003). Depending on the problem at hand, accurately capturing such pre-asymptotic/anomalous behavior is critical.

While anomalous transport is commonly observed in single-phase flows, its signatures can be even stronger in multiphase systems. Anomalous transport signatures are known to become stronger as greater geometrical complexity, such as boundary roughness or secondary porosity is resolved (Bijeljic et al. 2013a, b). The presence of a trapped phase has a similar effect, altering the connectivity and complexity of available flow paths. Depending on how the trapped phase distributes itself, this could lead to enhanced preferential flow paths or a larger number of trapping regions, both of which would result in enhanced spreading. Indeed several studies report enhanced dispersion in porous media as the saturation of the medium decreases (e.g., Wildenschild and Jensen 1999; Nützmann et al. 2002; Sato et al. 2003; Raoof and Hassanizadeh 2013) and stronger non-Fickian signatures have been reported (e.g., Bromly and Hinz 2004; Guillon et al. 2013). For example, Guillon et al. (2013) report

that they experimentally observe weak anomalous behavior ($\beta = 1.17$) in a single-phase experiment in a homogeneous column, but that the system becomes strongly anomalous $\beta = 1.5$ during a steady-state two-phase (oil-water) experiment in the exact same column. Such effects haven been shown to have a profound effect on mixing and reaction processes in both two- and three-phase systems Jiménez-Martínez et al. (2015, 2016), where rates of mixing are significantly faster than in a single-phase counterpart system. However, such behaviors may not be universal and observations have also been made that suggest the opposite—that dispersion can increase as saturation increases and approaches the single-phase limit (e.g., Vanderborght and Vereecken 2007). In these cases, the proposed mechanism is that enhanced saturation is associated with enhanced flow rates, which in turn gives rise to a broader distribution of velocity scales.

From the above discussion, it should be clear that multiphase flows in porous media and the transport of any associated dissolved substances can display a very rich and interesting set of dynamics and that many open questions still remain. For example, when the trapped phase distributes itself and creates preferential flow paths and a greater number of trapping regions, is the multiphase nature of the flow important? That is, does this trapped phase merely act in a similar manner to having an increased amount of solid matrix? Or, is the fact that the interface between the flowing and trapped phases is not a no-slip boundary important? Kazemifar et al. (2016) experimentally showed the emergence of strong recirculation zones near such interfaces, and recirculation zones have been speculated as contributors to anomalous dispersion (Le Borgne et al. 2011; Bolster et al. 2014). Another important question, given that the trapped phase can create regions of greater trapping, is how the initial condition associated with the dissolved substance impacts any anomalous behavior. For example, is it important to account for whether one starts in a highly mobile or immobile region (Singha et al. 2007)? This might have important consequences, as laboratory and field experiments might typically inject tracers into the more mobile regions of a flow, while processes of interest might be associated with regions of lower mobility (e.g., dissolution of trapped CO_2 into brine (Iglauer 2011)). Similarly, while enhanced non-Fickian dispersion might be expected in a multiphase system, one should also ask if the transition time from pre-asymptotic to asymptotic dispersion is similar for a comparable single and multiphase system ($O(L^2/D)$)? A priori one might anticipate them to be, as long as the characteristic length of the system is the same.

In this paper, through the use of numerical simulations, we explore the above questions with the goal of providing further insights into transport processes in multiphase systems. In Sect. 2, we describe the flow domain and methods by which we simulate flow and transport in it as well as the observables that we measure to answer the above questions. In Sect. 3, we present and discuss the results of the numerical simulations. We finish with conclusions in Sect. 4.

2 Model System

2.1 Solid Geometry

Our 2D solid geometry was artificially generated to produce a random range of pore configurations and sizes, while respecting a minimum pore diameter deemed necessary for sufficiently accurate fluid flow calculations. The resulting pore domain is fully periodic and also exhibits a wide variety of grain sizes and shapes. The generation process involved randomly placing solid phase circles of radius 10 onto a periodic region 1024×512 pixels in size. Each new circle of solid phase was tested for compatibility with the existing pore structure, and if successful, any void-space pixels within the test circle were converted to solid phase pixels. Any

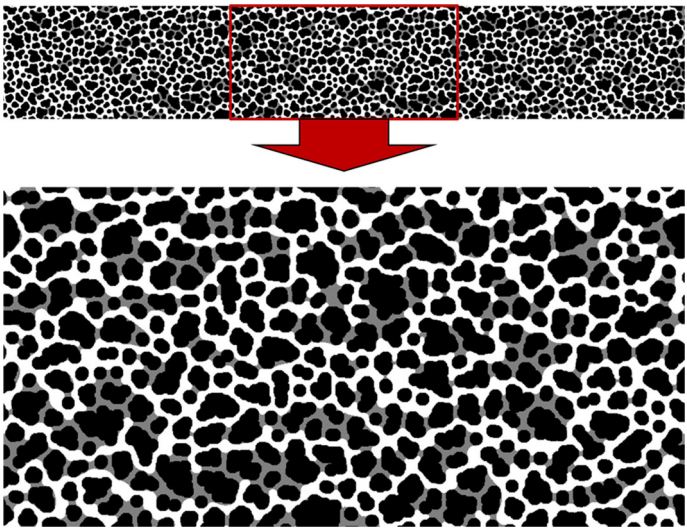

Fig. 1 Large tiled and small flow domain geometry with phase distributions

circle that did not lie within 6 pixels of any existing solid space was immediately allowed. For each new circle within 6 pixels of existing structure, we considered the shape of existing solid phase within an *outer* concentric circle of radius 16. If this existing solid phase was (i) simply connected and (ii) intersected an *inner* concentric circle of radius 9, with the intersection also being simply connected, the circle was allowed. Circles of solid phase were tested and added until the porosity of the region reduced to 40%. In this manner, we were able to adequately produce a random solid geometry and simply connected pore space compatible with efficient flow calculations, as illustrated at the bottom of Fig. 1.

Before any consideration of multiphase flow, our porous domain contains 46292 edges between solid and void cells and a total of 209700 void cells. Including a factor of $(1 + \sqrt{2})/(2\sqrt{2})$ to correct for diagonal pore walls, and comparing the edge to area ratio of straight, uniform pores then suggests an average pore size of 10.61. The length of the periodic region is approximately 100 times the average pore size, and the width approximately 50 times the average pore size.

2.2 Flow

The flow state inside the porous medium is complex because of the heterogeneous medium structure and the existence of multiphase fluids. We calculate both single-phase and multiphase flow behavior using direct simulation methods on the generated artificial porous media. The complex flow is solved using the lattice Boltzmann method (LBM), which because of its flexibility and ability to handle complex boundaries has many practical advantages in the context of multiphase flows in porous media (e.g., Jiang and Tsuji 2017; Ramstad et al. 2012).

We first carried out a drainage simulation to obtain a realistic spatial distribution of trapped phase. For this purpose, we adopted the improved Rothman-Keller (RK) multiphase lattice Boltzmann model which is able to reduce the lattice pinning effect (Latva-Kokko and Rothman 2005; Leclaire et al. 2012). This RK model is briefly introduced as follows: In LBM,

a discrete particle distribution function (PDF) f_i is introduced to represent the fluid. Here, i represents the ith lattice direction. For two-dimensional simulation, the two-dimensional 9 velocity lattice model (D2Q9) Qian et al. (1992) is employed in this work. For two-phase systems, the PDF for fluid k is denoted by $f_i^k (k = 1, 2)$. The total PDF at $(\mathbf{x}, t)$ is

$$f_i(\mathbf{x}, t) = \sum_k f_i^k(\mathbf{x}, t). \tag{1}$$

The lattice Boltzmann equation for fluid k is

$$f_i^k(\mathbf{x} + \mathbf{e}_i \delta t, t + \delta t) = f_i^k(\mathbf{x}, t) + \Omega_i^k(\mathbf{x}, t), \quad k = 1, 2, \quad i = 0, \ldots, 8 \tag{2}$$

where $\mathbf{e}_i$ is the lattice velocity of the D2Q9 model and $\Omega_i^k(\mathbf{x}, t)$ is the collision operator, which is a result of the combination of three suboperators in the RK mode (Tölke 2002; Jiang and Tsuji 2017):

$$\Omega_i^k = (\Omega_i^k)^3[(\Omega_i^k)^1 + (\Omega_i^k)^2] \tag{3}$$

where $(\Omega_i^k)^1$ is the usual single-phase collision operator, $(\Omega_i^k)^2$ is the multiphase perturbation operator responsible for the generation of interfacial tensions, and $(\Omega_i^k)^3$ is the multiphase collision operator for recoloring, which mimics the phase segregation. The detailed expressions for these collision operators can be found in Jiang and Tsuji (2017). The macroscopic variables (density ρ and velocity $\mathbf{u}$) can be calculated from the PDF:

$$\rho_k = \sum_i f_i^k, \quad \rho\mathbf{u} = \sum_i \sum_k f_i^k \mathbf{e}_i. \tag{4}$$

As the LBM is a Cartesian-based method, each pixel of the generated geometry directly corresponds to a mesh grid of the computational domain. To simulate the drainage process, we injected non-wetting phase fluid to displace the in-situ saturated wetting phase. A larger porous simulation region was created by tiling our periodic domain three times longitudinally. As part of the drainage simulation, two buffer layers 10 pixels in width were added at the inlet and outlet (longitudinal boundaries) of the tiled sample for injecting and withdrawing fluid. Initially, only the inlet buffer layer was saturated with non-wetting phase, while other spaces were saturated with wetting phase. A constant pressure gradient is applied to drive the non-wetting phase into the pore space from the inlet buffer layer. For simplicity, both the density and viscosity of the two fluids were set to be identical, and wetting properties of the porous media were set such that the wetting phase perfectly wets the solid. The wetting property is modeled by assigning the value of the order parameter of RK model on the solid boundary nodes (Jiang et al. 2014). A no-slip bounceback boundary condition was applied at fluid-solid interfaces (Chen and Doolen 1998), while periodic boundary conditions were applied on external domain boundaries. The average capillary number $Ca = \frac{\mu U}{\sigma}$ was around 10^{-5}. The dynamic viscosity μ and surface tension σ are set to 1/6 and 0.03, respectively, in lattice units (lu). Lattice units are dimensionless units that incorporate a unit length measure equal to the size of an LBM grid cell and a unit time measure equal to the simulation time step. The average velocity U can be obtained from the simulation results. The simulation was stopped once the average flux rate and phase saturation adequately converged to steady-state values, meaning that capillary pressure had halted accumulation of non-wetting phase liquid in the pore space. Fig. 2 illustrates this drainage simulation at different times.

The final stage of our multiphase flow simulation involved extracting the center tile as in Fig. 1 and running an additional two-phase LBM simulation with fully periodic boundary conditions (and all physical parameters maintained at the same values as for the drainage

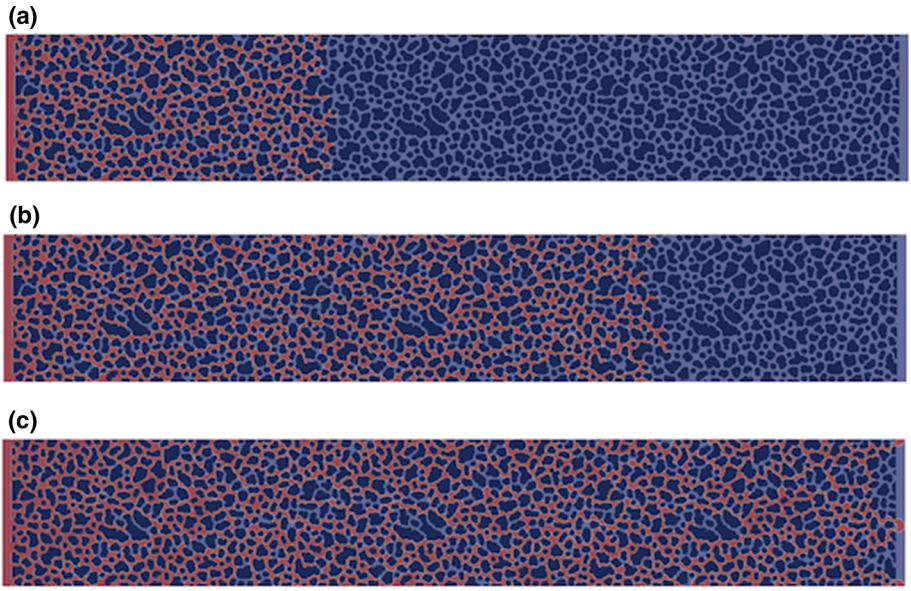

Fig. 2 Simulation of the drainage process

process). In this manner, we generated a natural, fully periodic stable fluid phase distribution exhibiting immobile wetting phase within a solid porous matrix.

For numerical studies of multiphase flow scenarios, the flow velocity field near interfaces suffers severely from unphysical spurious velocities and while some methods are less susceptible than others, it is a problem inherent to all multiphase flow solvers (Connington and Lee 2012). To avoid these spurious velocities affecting our particle tracking simulations, we conducted additional one-phase flow simulations using the fixed phase distribution shown at the bottom of Fig. 1, instead of directly using the velocity field obtained from multiphase flow simulation. In this approach, the flow is solved only for the invading phase. Strictly speaking, this means that we are not explicitly modeling transport in a multiphase flow, but rather a single-phase flow where we treat the trapped phase as a component that modifies the connectivity and interfacial slip of the mobile phase.

In two-phase flow, the trapped wetting phase induces an effective boundary slip length which will vary along each fluid-fluid interface and depends on the complex local geometry. The physical region occupied by each pocket of trapped phase is constant in time, but the trapped phase itself still exhibits internal circulation due to contact with the mobile fluid phase. Nonzero tangential velocities at fluid–fluid interfaces are equivalent to a varying boundary slip length when focussing solely on the mobile one-phase flow. Note that the minimum pore size in our artificial domain is approximately 6, and fluid–fluid interfaces typically occur spanning small pore throats or as thin layers over rougher grain surfaces. Schönecker and Hardt (2013) consider effective slip length estimation over rectangular cavities filled with immiscible fluids and adopt the distance to the center of the first in-cavity vortex as an upper bound on the maximum boundary slip length. For rectangular cavities, known one-phase flow solutions (Pan and Acrivos 1967; Higdon 1985) suggest a maximum in-cavity vortex distance of 0.25 times the width of the cavity. While the cavities containing trapped fluid are not rectangular in the present study, we can adopt similar reasoning to anticipate effective slip

lengths. Hence a slip length of 3 was estimated as an approximate upper bound for the variable slip length that would be induced at the majority of fluid–fluid interfaces in our domain for genuine two-phase flow. A constant slip length of 3 is imposed at *all* slip boundaries in our one-phase flow simulations so as to conservatively exaggerate any slip-induced effects on dispersion. We note that immiscible fluids can appear to exhibit slip at fluid-fluid boundaries of the order of a few molecular lengths in genuine two-phase flow simulations (Galliero 2010; Hu et al. 2010). We assume that our system length scales are large enough so that these effects do not invalidate the estimation above.

Computationally, the irregular curved slip boundaries were implemented using an ad hoc kinetic boundary condition (Singh et al. 2017) and the slip length was adjusted to equal 3 by artificially manipulating the Knudsen number [i.e., adjusting the relaxation time τ (Singh et al. 2017)] of single-phase simulation. To test this approximation and investigate whether dispersive behavior results from slip effects or the induced highly complex flow network, we tested three slip scenarios:

- *No slip*: imposing a non-slip boundary condition on all fluid–fluid interfaces (equivalent to converting the trapped wetting phase to solid phase).
- *Slip*: introducing an exaggerated proxy for two-phase flow by imposing a slip length of 3 at fluid-fluid boundaries while retaining the non-slip condition on solid-fluid boundaries.
- *Full slip*: a slip length of 3 was adopted at all boundaries including the solid-fluid boundaries. This case was included for completeness. Physically, we expect realistic two-phase flow behavior to lie somewhere between the *No slip* and *Slip* boundary conditions above.

Fully periodic one-phase LBM velocity fields were produced for each of the cases above. As expected, we observed higher velocities and a greater permeability for *Slip* versus *No slip* boundary conditions due to the increased boundary area (solid-fluid) with slip condition as illustrated in Fig. 3. Measured in lattice units, the average velocity in the flow direction was approximately 2.20×10^{-3}, 2.30×10^{-3} and 3.54×10^{-3}, respectively, for the *No slip*, *Slip* and *Full slip* flow scenarios. The final one-phase velocity fields of the three scenarios were used as inputs for particle tracking simulations investigating dispersion under various conditions.

For further comparison, we also considered pure one-phase flow in our artificial porous domain—that is, flow without any trapped wetting phase present, so that the non-wetting phase occupies the entire pore space (40% of the total volume). For scenarios described above where the trapped wetting phase is present, it occupies approximately 10% of the total volume, so that the non-wetting phase occupies the remaining 30% of the total volume. Without any trapped wetting phase present, we were able to consider one-phase *No slip* and *Full slip* LBM velocity fields, depending on whether a slip length of 0 or 3, respectively, was imposed on solid-fluid interfaces.

2.3 Particle Transport

To analyze transport of substances in solution, we implement a random walk (Risken 1996), where the plume is discretized into N particles, whose positions change at each time step according to both the local advective flow field and a constant applied diffusivity. For particle tracking, the lattice unit length scale L is retained, but a new timescale adopted so that the dimensionless average fluid velocity U is equal to one for all slip scenarios. Dimensionless time is then consistently related to the average distance travelled within the pore matrix by the mobile phase fluid. Much of the original void space is subsequently made inaccessible by trapped wetting-phase fluid, and hence, we should reconsider the average pore size stated in

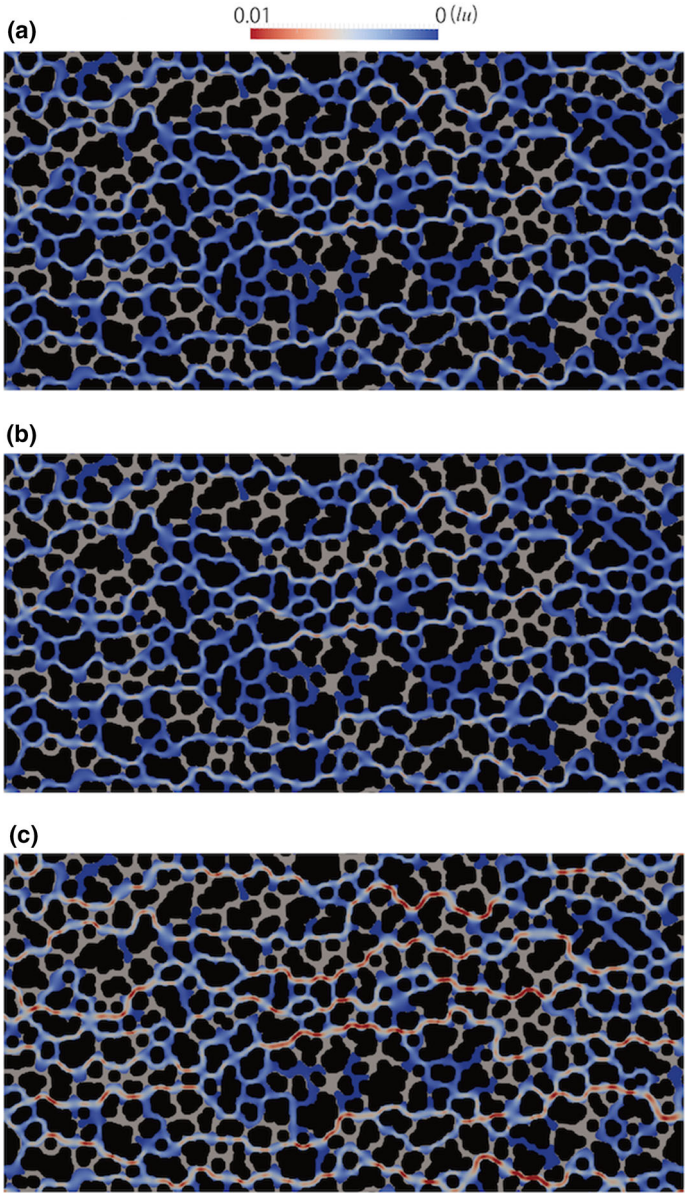

Fig. 3 Velocity fields inside pore spaces—comparison of different slip scenarios: **a** *No slip* **b** *Slip* **c** *Full slip*. Average horizontal velocity was approximately 2.20×10^{-3}, 2.30×10^{-3} and 3.54×10^{-3}, respectively, for the *No slip*, *Slip* and *Full slip* flow scenarios. Black and gray colors indicate the grains and trapped phase, respectively,

Sect. 2.1. Recalculating for the final area occupied by the mobile fluid gives a new average pore size of 10.05, which is very similar to the original value of 10.61. In summary, rescaling means that on average, the mobile fluid travels the average pore size in time $t \sim 10$ and traverses the entire domain in time $t \sim 10^3$. As our domain and flow fields are fully periodic, this poses no restriction, and results show maximum simulation times greater than $t = 2\times10^6$; with tracer particles typically traversing the domain length 2000 times.

The appropriate dimensionless value of the diffusivity coefficient D depends on temperature, pressure, pore size, capillary number and particle size; hence, we consider dimensionless $Pe = UL/D$ over four orders of magnitude from 0.1 to 100.

For a time step Δt, particle i moves as

$$\begin{aligned} \widehat{x}_i(t+\Delta t) &= \widehat{x}_i(t) + \widehat{u}_i\,\Delta t + \xi_i\sqrt{2\Delta t/Pe} \\ \widehat{y}_i(t+\Delta t) &= \widehat{y}_i(t) + \widehat{v}_i\,\Delta t + \eta_i\sqrt{2\Delta t/Pe} \end{aligned} \quad i = 1, ..., N\ , \tag{5}$$

where $\widehat{x}_i$ and $\widehat{y}_i$ are the horizontal and vertical position of particle i, respectively, $\widehat{u}_i$ and $\widehat{v}_i$ are the horizontal and vertical components of the normalized local fluid velocity, and ξ and η are independent identically distributed Gaussian variables with zero mean and unit variance.

The detailed advective flow field and domain for particle migration were derived from the LBM described above. Implementation of one approach is illustrated in Fig. 4. We calculated a 2048 × 1024 array of velocities by adding supplementary nodes (illustrated as crosses) to the original LBM nodes (illustrated as circles). All supplementary nodes adjacent to original solid phase nodes were defined to be of zero velocity. Velocities at all other supplementary nodes were determined according to the mean velocity of the two or four immediately adjacent original nodes. Migrating particles were elastically reflected from the derived region of identically zero flow (shaded in Fig. 4). The local velocity at all points not in the zero-flow region was determined via linear interpolation from the four immediately adjacent original or supplementary nodes.

Random walk particle tracking results were also obtained via independently authored code that incorporated diffusion via a single jump of fixed size at each time step, rather than Gaussian jumps. Velocities were alternatively obtained solely via linear interpolation

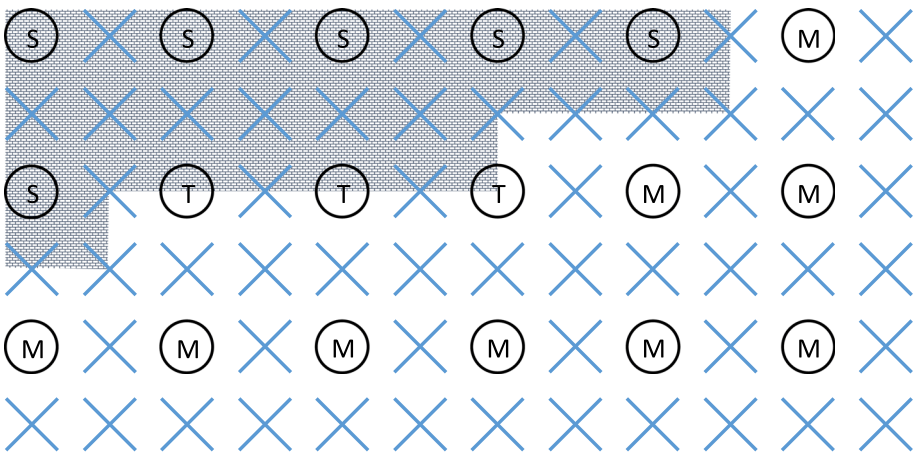

Fig. 4 Advective flow region for random walk particle migration. Circles represent LBM simulation nodes with associated phases solid (S), trapped (T), and mobile (M). Crosses show supplementary nodes. Particles reflect off the shaded zero-flow region

between the 1024×512 original nodes, avoiding the computational expense associated with the supplementary nodes of Fig. 4. The results for alternative particle tracking codes were found to be indistinguishable, and hence, final results were derived using the faster codebase.

Macroscopic dispersive behavior is affected over extended time periods by initial particle positions, especially when the flow network complexity incorporates stagnant fingers of fluid that act to trap tracer particles. We adopt two contrasting initial particle arrangements:

- Fast volumetric: initial positions chosen at random, with initial speed greater than 0.1 times the scaled average speed using the *No slip* flow field
- Slow volumetric: initial positions chosen at random, with initial speed less than 0.1 times the scaled average speed using the *Full slip* flow field

Particles can also be released after being randomly arranged on a line perpendicular to the flow direction. Results for such initial conditions are basically compatible with the volumetric initial conditions described above, and depend on whether the line of release incorporates fast flow regions or stagnant fingers of fluid.

2.4 Measure of Anomalous Transport - Second Centered Moment

The primary observable, which we calculate in our numerical simulations, is the temporal evolution of the second centered moment of the particle plume $\kappa_{11}(t)$, pinned to the longitudinal starting positions of the particles. Deviation from a diffusive scaling of this second centered moment (i.e., $\kappa_{11} \sim t^{\beta}$, $\beta \neq 1$) is widely regarded as the signature of anomalous transport. To calculate it, we calculate the first and second moments according to

$$m_1(t) = \sum_{i=1}^{N} \Big(x_i(t) - x_i(0) \Big), \qquad m_2(t) = \sum_{i=1}^{N} \Big(x_i(t) - x_i(0) \Big)^2, \tag{6}$$

which are combined as follows to calculate the second centered moment

$$\kappa_{11}(t) = m_2(t) - [m_1(t)]^2 \tag{7}$$

Choosing the total number N of particles to be tracked was a balance between obtaining sufficiently smooth and reproducible $\kappa_{11}(t)$ curves, and managing the significant computational expense associated with particle tracking. Curves in the results section were obtained using 1000 particles.

Using all of the above, we consider the evolution of $\kappa_{11}(t)$ for particle transport subject to four different diffusivities, two contrasting particle starting positions, and five different advective flow fields obtained by varying slip boundary conditions and the presence of trapped, wetting-phase fluid.

3 Results

3.1 The Role of Interface Boundary Condition

We firstly seek to investigate whether anomalous dispersion in the presence of trapped wetting phase is influenced by the induced slip boundary condition on fluid–fluid interfaces, or whether such dispersion is primarily the result of the induced complex flow geometry.

Figures 5 and 6 compare the evolution of $\kappa_{11}(t)$ under different slip boundary conditions on a log–log scale. When the $\kappa_{11}(t)$ curve is parallel to the $\beta = 1$ curves, we have standard

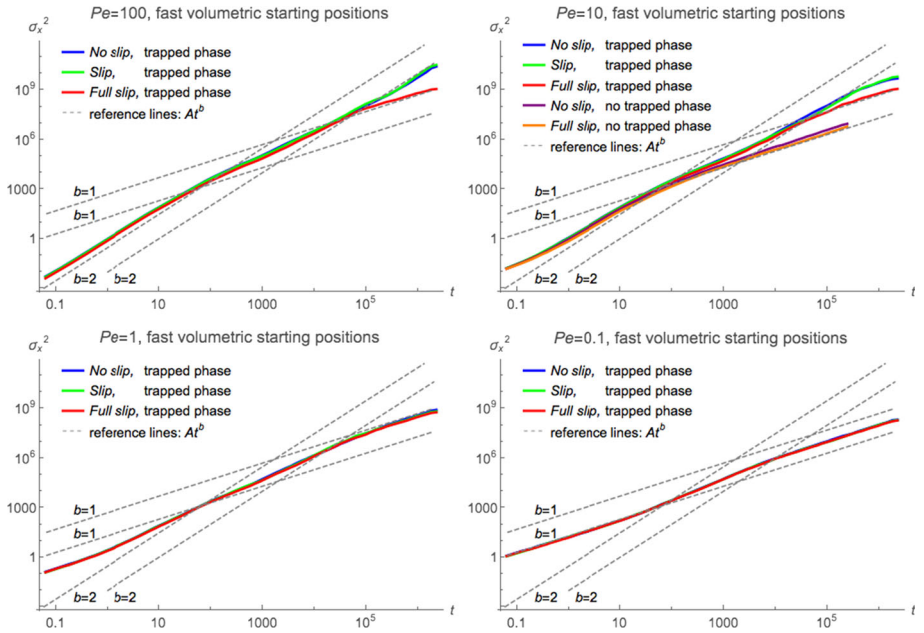

Fig. 5 Fast volumetric dispersive behavior with differing slip scenarios at various Peclet numbers

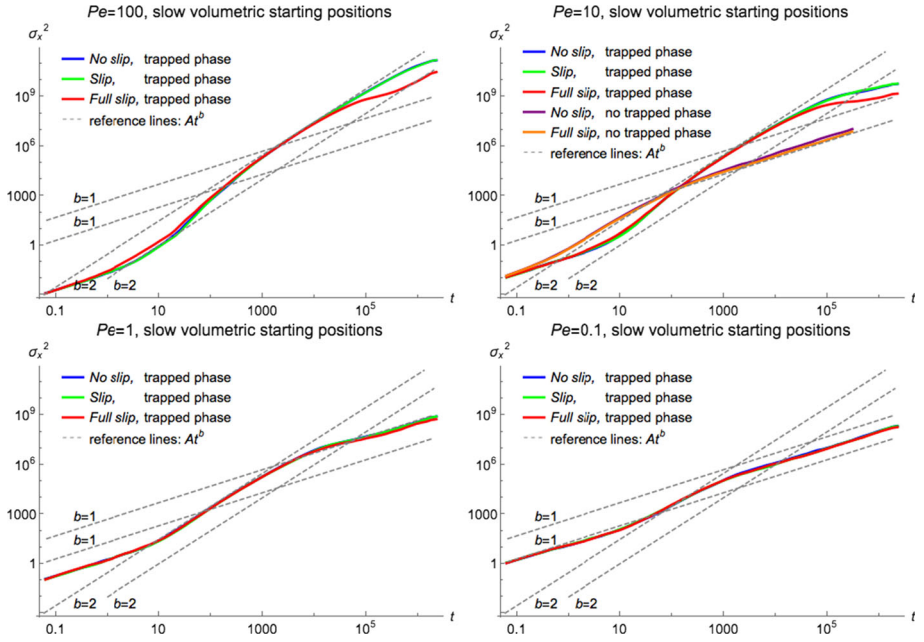

Fig. 6 Slow volumetric dispersive behavior with differing slip scenarios at various Peclet numbers

Fickian dispersion. Conversely, if the illustrated $\kappa_{11}(t)$ curve is parallel to the $\beta = 2$ curves, our observed dispersion is extremely superdiffusive. Eight different subplots are shown for fast and slow volumetric starting positions and varying Pe values. In all cases, there appears to be no observable difference between the *No slip* and standard *Slip* flow fields in the presence of trapped wetting phase fluid, suggesting that indeed the trapped phase acts in such a way as to restrict the flow paths in the same manner as the solid matrix.

Results for the *Full slip* flow field with trapped wetting phase are also shown and clearly affect $\kappa_{11}(t)$ for larger times compared to the other two slip scenarios. Although research has demonstrated that slip conditions are possible under certain circumstances (e.g., highly polished surfaces, very dilute gas flow), from most practical perspectives the *Full slip* flow field is essentially unphysical, but nonetheless is interesting and demonstrates that extreme slip boundary conditions can affect macroscopic dispersion. In particular, at late time the dispersion is reduced relative to the other two cases, presumably reflecting a narrower distribution of velocities to be sampled.

The fast and slow volumetric starting positions lose much of their intended distinctiveness for particle migration simulations using flow fields that lack trapped wetting phase. Nonetheless, results are shown for the $Pe = 10$ case. For both starting positions, the transition to post-asymptotic Fickian dispersion appears to happen quickly at approximately $t = 10^2$ to $t = 10^3$, corresponding to a typical longitudinal particle migration of about one domain length. Notably, such a transition appears to happen two to three orders of magnitude in time later for the flows with trapped phase present, despite the fact that the flow domain is still of the same size. Thus, the presence of the trapped phase significantly enhances the time and distance over which the system loses the memory of its initial condition and attains an asymptotic Taylor dispersion regime, as one would expect of any periodic flow domain.

3.2 The Role of Microscale Diffusion Coefficient

It is clear that the assumed Peclet number Pe greatly influences the severity and duration of anomalous dispersion shown by the plots of $\kappa_{11}(t)$ already introduced. At very low molecular diffusivity, particles essentially follow advective flow streamlines and can hence experience extended times stalled in stagnant flow regions, or alternatively can be carried forward large distances over relatively small times when positioned in fast flow regions. This slows the homogenization necessary for the transition to asymptotic Fickian dispersion, and may increase the severity of anomalous dispersion observed in the pre-asymptotic regime. High molecular diffusivities cause particles to frequently migrate between flow streamlines: Particles in stagnant regions of the advective flow can more easily escape due to diffusive motion, and particles in high flow streamlines are less likely to remain there for long enough to cover large distances.

The influence of Pe is more clearly observed in our results by fixing both the background advective flow field and particle starting positions while varying only the assumed molecular diffusivity. Fig. 7 shows this variation with Pe for four scenarios involving either *Slip* or *Full slip* velocity fields in the presence of trapped wetting phase, and either fast or slow volumetric starting positions. As observed above, our obtained evolution of $\kappa_{11}(t)$ for *No slip* advective flow is essentially equivalent to results for *Slip* advective flow, and hence, the two left panels of Fig. 7 also indicate the effect of Pe in our *No slip* advective flow field. Subplots of Fig. 7 with fast volumetric starting positions show that larger values of Pe delay the onset of superdiffusive behavior: It takes longer for the effects of the advective background flow to become apparent. This is not as evident for slow volumetric starting positions as many

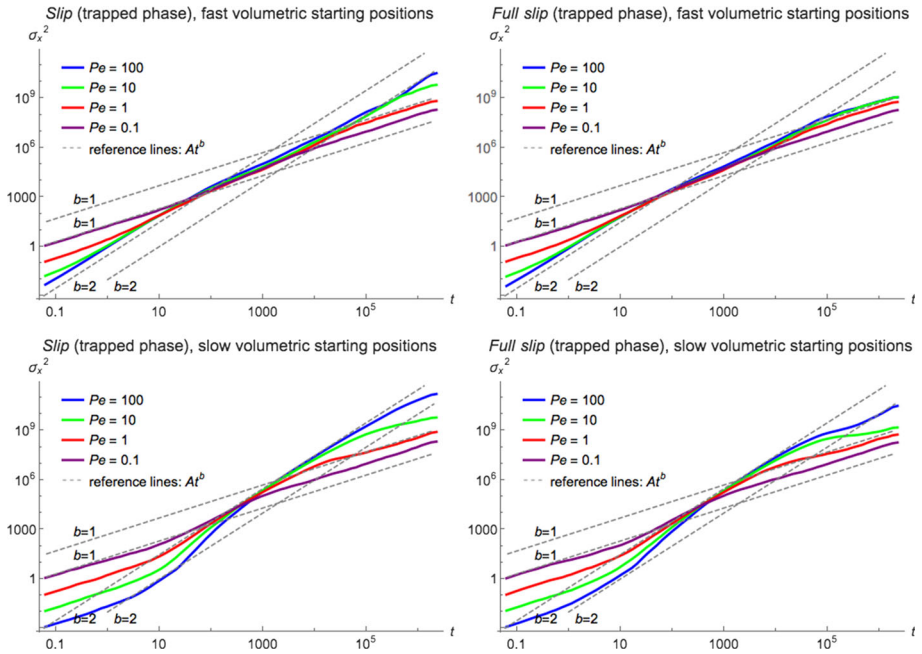

Fig. 7 Fast volumetric dispersive behavior with differing slip scenarios at various Peclet numbers

particles begin their migration in stagnant fingers of fluid where the background fluid velocity is largely absent. For $Pe = 1$, and 10, the large-time approach to Fickian diffusive spreading is apparent. The convergence to Fickian behavior is delayed as D decreases, and not observed at all in our results for $Pe = 100$.

While not clearly apparent from the fast volumetric subplots, the severity of the anomalous dispersion observed also increases with decreasing molecular diffusivity. The slow volumetric starting positions exhibit periods of extreme superdiffusion with $\beta > 2$, as well as brief periods of apparent subdiffusive flow where $\beta < 1$. These striking effects arise because of many particles beginning their migration from something comparable to a trapped state. This causes an artificially long-tailed distribution of tracer particles at intermediate times.

3.3 The Role of Initial Condition of Particles

We can better observe the effects of varying tracer particle starting positions by producing plots with the velocity field and Pe held constant, as in Fig. 8. Again, only *Slip* and *Full slip* velocity fields with trapped phase present are considered.

For sufficiently small values of Pe (0.1 and 1), we confirm that the properties of our starting positions do not matter for sufficiently large times and that all signatures of the initial condition are washed out. However, the initial conditions do affect the temporal evolution of $\kappa_{11}(t)$ when anomalous dispersion is present at intermediate times. For large values of Pe (10 and 100), the effects of our initial particle positions are evident even at the largest simulation times considered: $t \sim 2 \times 10^6$. As already described, having many particles start in stagnant fluid regions for the slow volumetric starting positions results in extreme superdiffusive behavior at various times, even faster than ballistic. This reflects the fact that

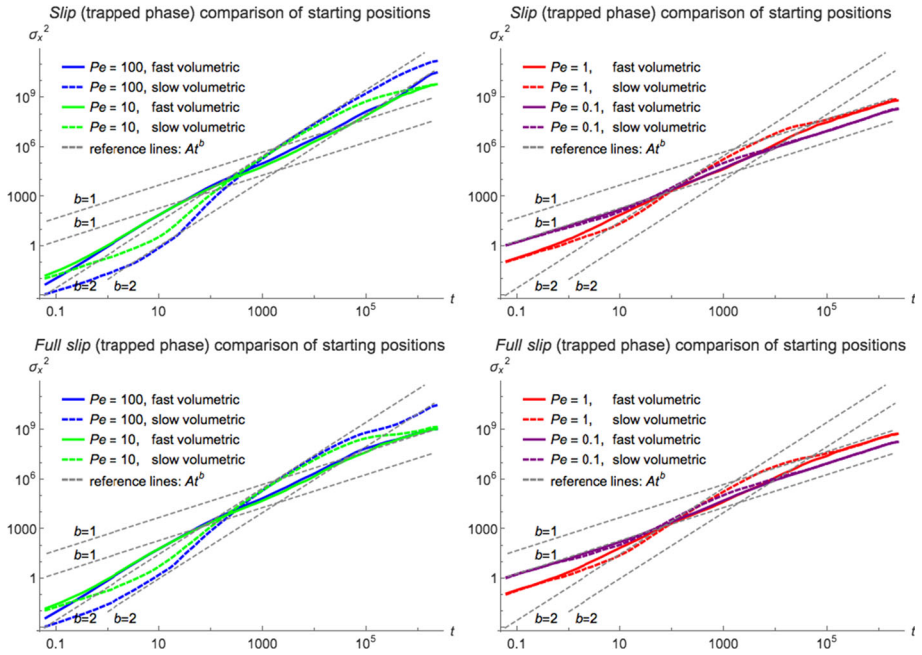

Fig. 8 Fast volumetric dispersive behavior with differing slip scenarios at various Peclet numbers

the velocity distribution sampled by the particles has not converged to its ultimate equilibrium (e.g., Dentz et al. 2016)

4 Conclusions

We have sought to increase our fundamental understanding of anomalous dispersion in two-phase porous media flow. In addition to demonstrating the surprising persistence of pre-asymptotic dispersion even for our relatively small periodic domain, our results directly illustrate the influence of the molecular diffusivity, tracer particle initial positions and slip at fluid–fluid interfaces.

Vast differences in the persistence and severity of upscaled anomalous dispersion result from assuming different values of the Peclet number Pe. Despite our simulated domain necessarily being periodic in nature, for large Pe we did not observe the final transition to Fickian behavior even after simulating particle migration for approximately 2000 domain lengths. Volume averaging and associate theories show that the time scale for this to happen is typically on the order of $\tau_D = L^2/D$. The fact that this behavior persists for much longer in the presence of the trapped phase suggests that the role of the trapped phase is to significantly increase this time scale, or seen otherwise increase the characteristic length scale of the medium by creating a more complex flow network with greater dead end channels and trapping structures. As our results show, it is not sensible to characterize the dispersive nature of flow in a porous system without specifying the molecular diffusivity. Researchers should be conscious of this when using particle-based methods; whereby, fluid particles are in fact

diffusing throughout the course of the simulation, possibly without the effective molecular diffusivity being explicitly acknowledged or quantified.

Especially in the presence of stagnant fluid regions where particles may be effectively trapped for significant periods of time, the initial positions of molecules transported via porous media flow have a significant effect on the nature of observed anomalous pre-asymptotic dispersion. Eventually, all dependence on initial conditions must fade away, but our simulation times were not sufficient to observe this for larger values of Pe. To ensure accurate results, researchers should be careful to choose physically appropriate initial conditions for pre-asymptotic model systems.

To avoid the currently unsolved issue of spurious velocities, we have utilized velocity fields derived from one-phase lattice Boltzmann simulations in the presence of a natural, fixed distribution of trapped wetting phase. These one-phase LBM simulations incorporate a constant slip length imposed at fluid–fluid interfaces, and no slip boundary conditions at solid-fluid interfaces. We expect that an accurate flow field for explicit two-phase flow would exhibit variable slip boundary conditions that correspond to an intermediary state between the *No slip* and *Slip* velocity fields that we have used. Our *No slip* and *Slip* velocity fields produce essentially the same macroscopic dispersion at all times considered, hence implying that induced slip at fluid–fluid interfaces does not affect anomalous dispersion in our system. Of course, numerical errors, even when small, can amplify and lead to discrepancies with reality, particularly given that the present numerical experiments span 7 orders of magnitude in time. However, the fact that we used two independently written and implemented random walk models to obtain virtually identical results gives some degree of confidence in the findings.

The implications for modeling of similar multiphase flows in porous media are that the important effects of persistent anomalous dispersion might be solely predicted from the induced flow geometry. Neglecting what previously would have been assumed to be an important physical boundary condition simplifies general analysis, and implies that better-developed tools for one-phase flows may at times be utilized.

Acknowledgements This research was made possible by a Kyushu University, International Institute for Carbon Neutral Energy Research (I^2CNER), Competitive Funding Initiative on Applied Math for Energy Project Grant. We would also like to express thanks for financial support via NSF Grants EAR-1351625, EAR-1446236 and CBET-1803989, as well as a JSPS Grant-in-Aid for Young Scientists (16K18331).

References

Bachu, S.: Sequestration of CO_2 in geological media: criteria and approach for site selection in response to climate change. Energy Convers. Manag. **41**(9), 953–970 (2000)

Berglund, S., Bosson, E., Selroos, J.O., Sassner, M.: Identification and characterization of potential discharge areas for radionuclide transport by groundwater from a nuclear waste repository in Sweden. Ambio **42**(4), 435–446 (2013)

Berkowitz, B., Cortis, A., Dentz, M., Scher, H.: Modeling non-Fickian transport in geological formations as a continuous time random walk. Rev. Geophys. **44**(2) (2006). https://doi.org/10.1029/2005RG000178

Berning, T., Djilali, N.: A 3D, multiphase, multicomponent model of the cathode and anode of a PEM fuel cell. J. Electrochem. Soc. **150**(12), A1589–A1598 (2003)

Bijeljic, B., Blunt, M.J.: Pore-scale modeling and continuous time random walk analysis of dispersion in porous media. Water Resour. Res. (2006). https://doi.org/10.1029/2005WR004578

Bijeljic, B., Mostaghimi, P., Blunt, M.J.: Insights into non-Fickian solute transport in carbonates. Water Resour. Res. **49**(5), 2714–2728 (2013a)

Bijeljic, B., Raeini, A., Mostaghimi, P., Blunt, M.J.: Predictions of non-Fickian solute transport in different classes of porous media using direct simulation on pore-scale images. Phys. Rev. E **87**(1), 013011 (2013b)

Bolster, D., Valdés-Parada, F.J., LeBorgne, T., Dentz, M., Carrera, J.: Mixing in confined stratified aquifers. J. Contam. Hydrol. **120**, 198–212 (2011)
Bolster, D., Méheust, Y., Le Borgne, T., Bouquain, J., Davy, P.: Modeling preasymptotic transport in flows with significant inertial and trapping effects-the importance of velocity correlations and a spatial Markov model. Adv. Water Resour. **70**, 89–103 (2014)
Bouwer, H.: Artificial recharge of groundwater: hydrogeology and engineering. Hydrogeol. J. **10**(1), 121–142 (2002)
Brenner, H.: Macrotransport Processes. Elsevier, New York (2013)
Bromly, M., Hinz, C.: Non-Fickian transport in homogeneous unsaturated repacked sand. Water Resour. Res. (2004). https://doi.org/10.1029/2003WR002579
Chen, S., Doolen, G.D.: Lattice Boltzmann method for fluid flows. Annu. Rev. Fluid Mech. **30**(1), 329–364 (1998)
Connington, K., Lee, T.: A review of spurious currents in the lattice Boltzmann method for multiphase flows. J. Mech. Sci. Technol. **26**(12), 3857–3863 (2012)
Daly, E., Porporato, A.: A review of soil moisture dynamics: from rainfall infiltration to ecosystem response. Environ. Eng. Sci. **22**(1), 9–24 (2005)
De Anna, P., Le Borgne, T., Dentz, M., Tartakovsky, A.M., Bolster, D., Davy, P.: Flow intermittency, dispersion, and correlated continuous time random walks in porous media. Phys. Rev. Lett. **110**(18), 184502 (2013)
Dentz, M., Le Borgne, T., Englert, A., Bijeljic, B.: Mixing, spreading and reaction in heterogeneous media: a brief review. J. Contam. Hydrol. **120**, 1–17 (2011)
Dentz, M., Kang, P.K., Comolli, A., Le Borgne, T., Lester, D.R.: Continuous time random walks for the evolution of Lagrangian velocities. Phys. Rev. Fluids **1**(7), 074004 (2016)
de Barros, F.P., Bolster, D., Sanchez-Vila, X., Nowak, W.: A divide and conquer approach to cope with uncertainty, human health risk, and decision making in contaminant hydrology. Water Resour. Res. (2011). https://doi.org/10.1029/2010WR009954
de Barros, F., Fernàndez-Garcia, D., Bolster, D., Sanchez-Vila, X.: A risk-based probabilistic framework to estimate the endpoint of remediation: concentration rebound by rate-limited mass transfer. Water Resour. Res. **49**(4), 1929–1942 (2013)
Fernández-Arévalo, T., Lizarralde, I., Grau, P., Ayesa, E.: New systematic methodology for incorporating dynamic heat transfer modelling in multi-phase biochemical reactors. Water Res. **60**, 141–155 (2014)
Galliero, G.: Lennard-Jones fluid-fluid interfaces under shear. Phys. Rev. E (2010). https://doi.org/10.1103/PhysRevE.81.056306
Gómez-Hernández, J.J., Butler, J., Fiori, A., Bolster, D., Cvetkovic, V., Dagan, G., Hyndman, D.: Introduction to special section on modeling highly heterogeneous aquifers: lessons learned in the last 30 years from the MADE experiments and others. Water Resour. Res. **53**(4), 2581–2584 (2017)
Guillon, V., Fleury, M., Bauer, D., Neel, M.C.: Superdispersion in homogeneous unsaturated porous media using NMR propagators. Phys. Rev. E **87**(4), 043007 (2013)
Higdon, J.J.L.: Stokes flow in arbitrary two-dimensional domains: shear flow over ridges and cavities. J. Fluid Mech. **159**, 195–226 (1985)
Hu, Y., Zhang, X., Wang, W.: Boundary conditions at the liquid-liquid interface in the presence of surfactants. Langmuir **26**(13), 10693–10702 (2010)
Iglauer, S.: Dissolution trapping of carbon dioxide in reservoir formation brine—a carbon storage mechanism. In: Mass Transfer — Advanced Aspects, InTech, pp. 233–262 (2011)
Jiang, F., Tsuji, T.: Estimation of three-phase relative permeability by simulating fluid dynamics directly on rock-microstructure images. Water Resour. Res. **53**(1), 11–32 (2017)
Jiang, F., Tsuji, T., Hu, C.: Elucidating the role of interfacial tension for hydrological properties of two-phase flow in natural sandstone by an improved lattice Boltzmann method. Transp. Porous Media **104**(1), 205–229 (2014)
Jiménez-Martínez, J., Anna, Pd, Tabuteau, H., Turuban, R., Borgne, T.L., Méheust, Y.: Pore-scale mechanisms for the enhancement of mixing in unsaturated porous media and implications for chemical reactions. Geophys. Res. Lett. **42**(13), 5316–5324 (2015)
Jiménez-Martínez, J., Porter, M.L., Hyman, J.D., Carey, J.W., Viswanathan, H.S.: Mixing in a three-phase system: enhanced production of oil-wet reservoirs by CO_2 injection. Geophys. Res. Lett. **43**(1), 196–205 (2016)
Kang, P.K., Anna, P., Nunes, J.P., Bijeljic, B., Blunt, M.J., Juanes, R.: Pore-scale intermittent velocity structure underpinning anomalous transport through 3-D porous media. Geophys. Res. Lett. **41**(17), 6184–6190 (2014)
Kazemifar, F., Blois, G., Kyritsis, D.C., Christensen, K.T.: Quantifying the flow dynamics of supercritical CO_2-water displacement in a 2D porous micromodel using fluorescent microscopy and microscopic PIV. Adv. Water Resour. **95**, 352–368 (2016)

Lake, L.W.: Enhanced Oil Recovery. Prentice Hall, Englewood Cliffs (1989)
Latva-Kokko, M., Rothman, D.H.: Static contact angle in lattice Boltzmann models of immiscible fluids. Phys. Rev. E **72**, 046701 (2005). https://doi.org/10.1103/PhysRevE.72.046701
Le Borgne, T., Bolster, D., Dentz, M., Anna, P., Tartakovsky, A.: Effective pore-scale dispersion upscaling with a correlated continuous time random walk approach. Water Resour. Res. **47**(12) (2011). https://doi.org/10.1029/2011WR010457
Leclaire, S., Reggio, M., Trépanier, J.Y.: Numerical evaluation of two recoloring operators for an immiscible two-phase flow lattice Boltzmann model. Appl. Math. Model. **36**(5), 2237–2252 (2012)
Mercer, J.W., Cohen, R.M.: A review of immiscible fluids in the subsurface: properties, models, characterization and remediation. J. Contam. Hydrol. **6**(2), 107–163 (1990)
Nützmann, G., Maciejewski, S., Joswig, K.: Estimation of water saturation dependence of dispersion in unsaturated porous media: experiments and modelling analysis. Adv. Water Res. **25**(5), 565–576 (2002)
Pan, F., Acrivos, A.: Steady flows in rectangular cavities. J. Fluid Mech. **28**(4), 643–655 (1967)
Qian, Y., d'Humières, D., Lallemand, P.: Lattice BGK models for Navier—Stokes equation. EPL (Euro. Lett.) **17**(6), 479–484 (1992)
Ramstad, T., Idowu, N., Nardi, C., Øren, P.E.: Relative permeability calculations from two-phase flow simulations directly on digital images of porous rocks. Transp. Porous Media **94**(2), 487–504 (2012)
Raoof, A., Hassanizadeh, S.: Saturation-dependent solute dispersivity in porous media: pore-scale processes. Water Resour. Res. **49**(4), 1943–1951 (2013)
Risken, H.: Fokker–planck equation. In: The Fokker–Planck Equation, Springer, pp 63–95 (1996)
Sato, T., Tanahashi, H., Loáiciga, H.A.: Solute dispersion in a variably saturated sand. Water Resour. Res. (2003). https://doi.org/10.1029/2002WR001649
Schönecker, C., Hardt, S.: Longitudinal and transverse flow over a cavity containing a second immiscible fluid. J. Fluid Mech. **717**, 376–394 (2013)
Schumer, R., Benson, D.A., Meerschaert, M.M., Baeumer, B.: Fractal mobile/immobile solute transport. Water Resour. Res. (2003). https://doi.org/10.1029/2003WR002141
Singh, S., Jiang, F., Tsuji, T.: Impact of the kinetic boundary condition on porous media flow in the lattice Boltzmann formulation. Phys. Rev. E **96**, 013303 (2017). https://doi.org/10.1103/PhysRevE.96.013303
Singha, K., Day-Lewis, F.D., Lane, J.: Geoelectrical evidence of bicontinuum transport in groundwater. Geophys. Res. Lett. **34**(12) (2007). https://doi.org/10.1029/2007GL030019
Sund, N., Bolster, D., Mattis, S., Dawson, C.: Pre-asymptotic transport upscaling in inertial and unsteady flows through porous media. Transp. Porous Media **109**(2), 411–432 (2015)
Taylor, G.: Dispersion of soluble matter in solvent flowing slowly through a tube. Proc. R. Soc. Lond. A Math. Phys. Eng. Sci. **219**(1137), 186–203 (1953)
Tölke, J.: Lattice Boltzmann simulations of binary fluid flow through porous media. Philos. Transact. R. Soc. Lond. A: Math. Phys. Eng. Sce **360**(1792), 535–545 (2002)
Vanderborght, J., Vereecken, H.: Review of dispersivities for transport modeling in soils. Vadose Zone J. **6**(1), 29–52 (2007)
Whitaker, S.: The Method of Volume Averaging, vol. 13. Springer, Berlin (2013)
Wildenschild, D., Jensen, K.H.: Laboratory investigations of effective flow behavior in unsaturated heterogeneous sands. Water Resour. Res. **35**(1), 17–27 (1999)
Wood, B.D.: Inertial effects in dispersion in porous media. Water Resour. Res. (2007). https://doi.org/10.1029/2006WR005790
Zhang, Y., Benson, D.A.: Lagrangian simulation of multidimensional anomalous transport at the MADE site. Geophys. Res. Lett. (2008). https://doi.org/10.1029/2008GL033222